EPJ Photovoltaics **16**, 19 (2025)

https://doi.org/10.1051/epjpv/2025007

Available online at:
www.epj-pv.org

Special Issue on 'EU PVSEC 2024: State of the Art and Developments in Photovoltaics', edited by Robert Kenny and Gabriele Eder

ORIGINAL ARTICLE OPEN ACCESS

New approach of PV and thermal modeling to develop feasible cooling solutions for PV in buildings

Iñaki Cornago[1,*,a], Mikel Ezquer[1,**,a], Francisco Javier Sorbet[1], Alicia Kalms[2], Gonzalo Diarce[3], Olatz Irulegi[4], and Fritz Zaversky[1]

[1] Solar Energy Technologies and Storage Dpt., National Renewable Energy Center (CENER), Sarriguren 31621, Spain
[2] Grid Integration, Electric Storage and Hydrogen Dpt., National Renewable Energy Center (CENER), Sarriguren 31621, Spain
[3] Energy Engineering Dpt., University of the Basque Country (UPV/EHU), ENEDI Group, Bilbao 48013, Spain
[4] Architecture Dpt., University of the Basque Country (UPV/EHU), CAVIAR Research Group, San Sebastián 20018, Spain

Received: 28 June 2024 / Accepted: 6 February 2025

Abstract. This work presents a straightforward Building Applied PhotoVoltaic-Thermal element, characterized by its ease of implementation, utilizing conventional photovoltaic modules and standard supporting structures to form a narrow air ventilation channel with the roof of the building. A comprehensive transient thermal model is developed using the Modelica modeling framework, which accurately calculates key parameters such as energy production, photovoltaic module temperatures, and air temperature at the channel exit. This model is validated through a three-month experimental campaign, during which the element performance aiming photovoltaic modules cooling is monitored. The results demonstrate excellent alignment between simulated and experimental data, even under highly variable meteorological conditions. This validation demonstrates the huge potential of the model for assessing the feasibility of such solutions in buildings across diverse locations. The model has been applied to evaluate the potential benefits of the element in a real commercial building scheduled for renovation as part of the European oPENlab project (https://openlab-project.eu). Three fan installations and control scenarios are assessed and compared to optimize the net annual energy balance, defined as the difference between photovoltaic energy generation and fan energy consumption. An optimized four-step control strategy emerges as the most effective, yielding a 2.3% increase in the net annual energy balance for the analyzed roof. Furthermore, simulations reveal substantial reductions in the operating temperature of photovoltaic modules, with a maximum decrease of 35 °C on a sunny summer day. This reduction can significantly enhance the durability of the modules, in addition to the achieved boost in energy production.

Keywords: BAPV-T / BIPV-T / PV-T modeling / Modelica / PV ventilation channel / PV durability

1 Introduction

Solar energy, particularly solar photovoltaics (PV), has experienced a remarkable growth in recent years, driven by the urgent need to decarbonize energy systems and supported by a significant decrease in module prices [1]. However, as solar generation expands, the availability of suitable space for solar installations is becoming increasingly scarce, particularly in urban areas, which is leading to explore further technological design options [2].

To remain competitive, solar technologies must maintain low costs per unit of energy and maximize energy generation per square meter. Although PV systems are widely used and commercially available, they face several barriers, such as limited conversion efficiency, dust accumulation, and high PV cell temperatures that can damage the cells [3]. This overheating issue is particularly relevant in Building Integrated PV (BIPV) and Building Applied PV (BAPV) due to three main reasons: (i) partial or total absence of wind cooling on the rear side; (ii) larger diurnal temperature variations; and (iii) more frequent partial shadow nearby obstacles such as chimneys, antennas, trees and taller buildings, which can lead to dangerous hot spots.

To address the issue of high PV cell temperatures, significant research has been conducted into various cooling techniques over the past decades [4]. This research has led to the development of hybrid PV-thermal (PV-T) collectors, which generate both electricity and useful thermal energy from the same aperture area, achieving

* e-mail: icornago@cener.com
** e-mail: mezquer@cener.com
[a] These authors contributed equally to this work.

higher overall efficiencies compared to standalone systems [5]. Additionally, PV-T systems can be easily integrated with other components, such as hot water storage tanks, heat pumps, or batteries, to maximize thermal and electrical energy outputs. This is particularly important since thermal demand still accounts for around 50% of total energy consumption worldwide, predominantly met by fossil fuels [6]. Consequently, PV-T represents a promising technology, especially in scenarios of high solar penetration and urban environments where both thermal and electrical energy demands are present, and efficient use of limited space is essential [3,4,7].

Among the various types of PV-T systems, air-based PV-T collectors use air as the working fluid to regulate the temperature of the PV cells. These collectors are primarily used for ventilation, space heating, and air-preheating [8]. They can be integrated into some types of roofs and building façades [9], or installed as independent components on flat roofs [10]. Moreover, they have a simpler structure and are easier to integrate with space heating systems compared to water-based PV-T collectors, resulting in lower capital costs [3]. Additionally, issues such as freezing, boiling and corrosion can be avoided since the working fluid is air, compatible with domestic space heating systems [11]. However, these systems also have drawbacks, such as the need for relatively larger volumes of storage, difficulties in sealing, and potential energy loss due to hot air leakage from collectors and pipelines.

A review of the technical literature on air-based PV-T systems reveals several studies focusing on optimizing air gaps to enhance air circulation and effectively cool PV arrays [12], developing thermal modeling tools to estimate operating PV temperatures prior to installation [13], and ensuring the optimal configuration of the system to reduce building energy requirements [3,14]. These studies confirm the potential of air-based PV-T technology through both simulations and experiments, but also highlight the need for continuous optimizations to improve performance and reduce costs. These requirements are reinforced with the fact that, despite their demonstrated potential, especially for residential and commercial buildings, only a modest number of manufacturers are producing PV-T collectors, and their market penetration remains limited [15,16].

When analyzing the main bottlenecks for the widespread commercialization of air-based PV-T collectors, various published reviews [3,4,7,17] agree on highlighting the following limitations: higher cost compared to side-by-side solar systems (PV and solar thermal (ST) collectors), lack of public awareness, product standardization, warranties, performance certification issues, and shortage of installation and training experiences. Specifically, the cost of PV-T collectors remains considerably higher than separate PV panels and ST collectors, hindering widespread implementation. Furthermore, while PV panels and ST collectors are mature and well-known technologies, hybrid PV-T collectors are less recognized by the public, limiting their adoption. Moreover, the heaviness and large thickness of standard PV-T collectors complicate their implementation on regular tilted roofs of buildings. All these studies conclude that more research is required to develop new, cost-competitive products that deliver thermal energy with simple, affordable designs, mitigate thermal and electrical losses, and ensure collector reliability and longevity. Additionally, recognized testing procedures and standards, along with demonstration projects, are needed.

To address these research gaps, this study proposes a BAPV-T element (see Fig. 1a) with a straightforward configuration and designed to optimize electric production. It is based on the formation of an air ventilation channel at the back side of the PV modules. This forced air ventilation system relies on common fans, maintaining simplicity and adaptability. The proposed configuration offers broader integration possibilities than typical PV-T collectors, along with easier maintenance, and can be easily upgraded to a BIPV-T system if desired.

The performed work entails the development of a comprehensive simulation model to design and evaluate the element performance. Apart from accurately predicting key parameters of the system, such as PV energy production, module temperature, and air temperature at the channel exit, it enables the assessment of different control strategies for the ventilation through the channel. This model has been validated with a three-month experimental campaign performed in a real-scale experimental setup.

The IWER building (www.edificioiwer.es), an industrial heritage building in the Rochapea neighborhood of Pamplona, Spain, is scheduled for renovation. A BIPV-T system is currently under evaluation as a pivotal component of the EU-funded oPENlab project (https://openlab-project.eu), which explores different innovative approaches with the overarching goal of leading the transition to positive energy neighborhoods. In this context, the developed model has been applied to the roof section of this building with the most favorable sun orientation and the potential benefits of incorporating the proposed BAPV-T element are presented, including the assessment of several ventilation control strategies. Finally, the main achievements of the work are discussed along with the next steps in this research to broaden the scope of the proposed element and its modeling.

2 Materials and methods

2.1 PV-T model

Modelica is a multi-purpose physical system modeling language that has been developed in an international effort in order to unify already existing similar modeling approaches and to enable developed models and model libraries to be easily exchanged. The concept is based on non-causal models featuring true ordinary differential and algebraic equations, i.e. differential-algebraic equation systems [18]. A Modelica tool reads the developed Modelica code, performs symbolic manipulations of equations and translates the model into numerical simulation code, using state-of-the-art algorithms developed for general application [19]. Thus, developed models and model libraries are exchangeable, i.e. can be read and simulated using different Modelica environments. Today, commercial as well as open-source Modelica environments are available [20,21].

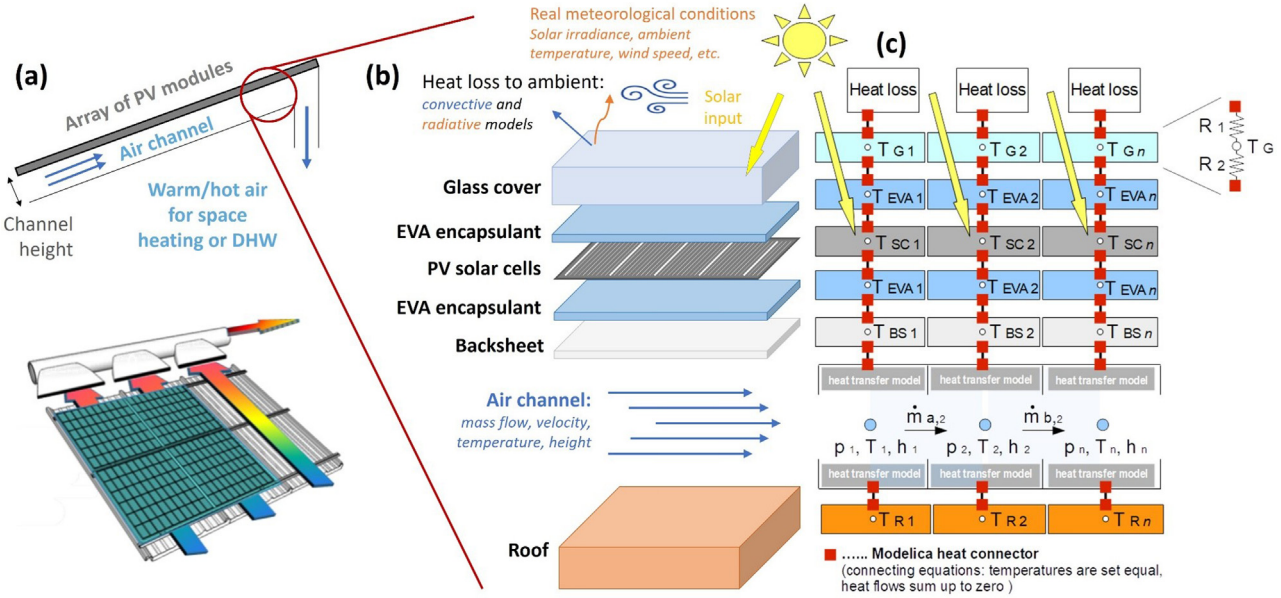

Fig. 1. Sketch of the BAPV-T system concept (a) with the multiple parameters and layers considered (b) and a detail of the discretized 1-D conductive model (c).

Table 1. Thermal and electrical parameters introduced into the model.

Thermal parameters			
Layer	Glass cover	Encapsulant	Backsheet
Thickness (mm)	3.20	0.46	0.29
Thermal conductivity (W/m·K)	1.33	0.33	0.29
Electrical parameters			
Maximum Power (STC)	Efficiency (STC)	Maximum Power Temperature coefficient	
P_{MPP} (W)	η (%)	γ (%/°C)	
385	20.9	−0.259	

Specifically, Modelica 4.0.0 version with Dymola 2022 simulation tool has been used to perform all the simulations of this study.

A comprehensive transient thermal model has been completely developed by CENER to evaluate the feasibility of the proposed BAPV-T installation. The element is modeled as several 1-D conduction layers connected to a 1-D flow model of the air channel (see Fig. 1c). The air channel below the PV module is modeled according to the finite volume method, based on the Modelica Standard Library [22]. The total flow volume is discretized in n finite control volumes (nodes) along the flow direction and mass and energy balances are solved in each control volume. Four nodes per module composing the air channel are used, ensuring convergence of simulation results. The PV module is modeled as layers of discretized 1-D conduction models where each node column of the conduction model is connected to corresponding node of the 1-D flow model (see Fig. 1c). The channel fluid model is linked to the 1-D conduction model array (PV module) via a convective heat transfer model based on the Newton's law of cooling (see Fig. 1c "heat transfer model"), which defines the relationship between the channel's inner surface temperatures, the fluid bulk temperatures (see Fig. 1c, T_1 to T_n) and the net heat flows of each control volume. The heat transfer coefficient is estimated using the well-known Gnielinski correlation [23].

As it can be seen in Figure 1b, the model takes into consideration thickness and thermal conductivity for each layer within a PV module, such as front glass, PV cell, top and bottom encapsulant layers, and backsheet, as well as the geometry of the air channel, and the air mass flow through it. Although the model can be applied to any kind of PV module, Meyer Burger Black modules with 385 W of nominal power are used in this study, as they have been initially selected within the oPENLab project for the PV installation assessed. The main electrical and thermal characteristics of this module are introduced into the model and are summarized in Table 1. Given the low thickness and high thermal conductivity of silicon relative to the other layers, the PV cell layer is considered negligible for the thermal conduction calculations in this model.

In addition, the model allows the integration of input parameters containing the main meteorological conditions, such as solar irradiance, ambient temperature, or wind speed, at any desired interval of time (e.g., hourly or every minute). Initially, the model calculates the solar heat inputs to the glass cover and PV cell using equations (1) and (2):

$$\dot{Q}_G = I_{PoM} \times S_{PV} \times A_G \tag{1}$$

$$\dot{Q}_{Cell} = I_{PoM} \times S_{PV} \times (1 - R_G - A_G) \times (1 - \eta) \tag{2}$$

where I_{PoM} is the irradiance in the plane of the modules; S_{PV} is the total area of the PV modules; A_G and R_G are the absorptivity and reflectivity of the glass cover, respectively; and η is the efficiency of the PV modules at the specific operating temperature, calculated according to equation (3) [24]:

$$\eta = \eta_{STC} - \eta_{STC} \times \gamma \times (T_{PV} - 25) \tag{3}$$

where η_{STC} is the module efficiency at Standard Test Conditions -STC- (irradiance 1000 W/m^2; temperature 25 °C; Air Mass 1.5 G); γ is the maximum power temperature coefficient of the modules (see Tab. 1); and T_{PV} is the operating temperature of the PV cells, calculated through thermal conductive sub-models considering convective and radiative heat losses to ambient, as well as modules cooling via the rear ventilation channel. The primary outputs of the model include the PV energy production, the temperature distribution of the modules along the length of the channel, and the air temperature at the channel exit.

Conventional rooftop PV installations have usually small air gaps between roof and backside of PV modules. Depending on the specific geometry and frame geometry of modules, a small contribution of convective cooling may be achieved. To compare the performance of the PV-T element with that of conventional rooftop PV installations, a low value of air velocity is set in the model, which represents the performance of a conventional rooftop PV system. This approach shall ensure a fair comparison of PV energy production between the proposed PV-T element and a conventional installation.

Finally, the simulation model integrates and evaluates the energy consumption of the fans responsible for providing a given air mass flow through the channel. This calculation was performed using the well-known equation (4) for fan or pump power consumption:

$$Power = \frac{Volumetric\ Flow \times Pressure\ Drop}{Efficiency} \tag{4}$$

where the volumetric flow is calculated from the air mass flow and the air density, and the pressure drop from the geometry of the channel and ducts. A conservative blower efficiency is assumed (50%), which would represent the lower bound. Depending on the total mass flow, type of blower and available funds, the efficiency can raise to about 65 to 70%.

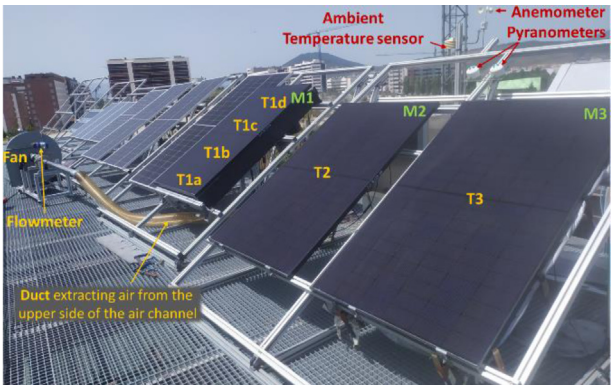

Fig. 2. Picture of the experimental setup installed on the roof of CENER headquarters, with one module with an air channel at the rear side (M1), a second module installed in a standard configuration (M2) and a third module thermally insulated at the back side (M3).

This way, the net energy balance is calculated as the difference between the PV energy generation and the energy consumption of the fans. This net energy balance serves as the figure of merit for the element design optimization.

2.2 Experimental setup

The specific experimental setup designed by CENER replicates a ventilation air channel at the rear side of one PV module (M1) and compares its performance with a second module (M2) installed in a field standard configuration. Since this configuration does not replicate a conventional rooftop installation, the comparison is complemented by a third module (M3) with its rear side thermally insulated. Three Meyer Burger Black modules (385 W of nominal power) are installed on substructures made of Bosch Rexroth profiles on the roof of CENER headquarters in Sarriguren, Spain (42° 48´33´´ N - 1° 40´55´´ W), tilted 32° in a south orientation to maximize direct solar radiation (see Fig. 2). Each of the monitored modules is electrically biased at the maximum power point (MPP) by using a Power Optimizer (SolarEdge P505), with the combined output connected to a monophasic PV inverter (SolarEdge SE4000H-RWS HD-WAVE).

The lateral walls of the air channel (M1) are also constructed using Bosch Rexroth profiles and completed with a methacrylate sheet at the rear, which is removable via profiles rails to allow flexibility for testing channel heights from 5 cm to 18 cm. The walls and rear side of the channel are insulated with a 13 mm Armaflex sheet to minimize thermal losses and replicate the installation of PV modules on a roof. A constant air mass flow through the channel is achieved using a CKAT/2-711 fan from Soler&Palau Ventilation Group, measured by a Krohne OPTISWIRL 4070/C flowmeter.

Operating temperatures of the modules are measured using calibrated thermocouples (model TC-type-T) adhered to the backsheet of the modules. M2 and M3

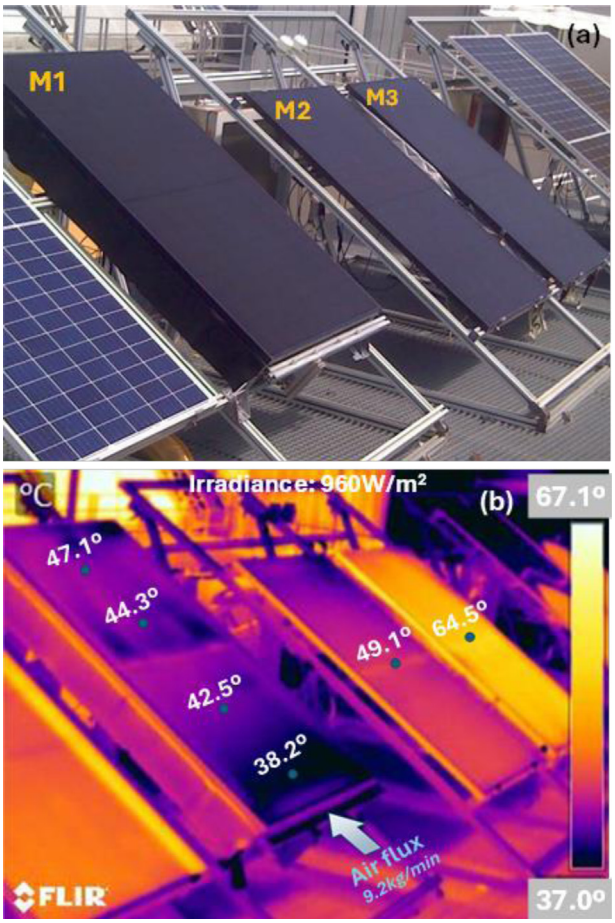

Fig. 3. (a) Photography of the three tested modules: module with air channel (M1), module in standard configuration (M2), and rear-insulated module (M3); (b) Infrared thermographic image under high irradiance conditions.

each have one thermocouple placed at the center, while M1 is equipped with four thermocouples to assess temperature variations along the channel due to potential air-cooling effects. In addition, temperatures at the modules front side are periodically measured using a thermographic camera (FLIR-E60) to instantly assess their thermal performance. The air is collected at the upper side of the channel through a duct connected to the fan, with its temperature and velocity at the exit of the channel measured using an anemometer (CTV 110 from Sauermann). The air temperature at the channel entrance is assumed to be the ambient temperature.

Meteorological conditions are monitored with a class-A pyranometer (EKO MS-80) to measure irradiance at the module plane, a temperature sensor (NRG 110S) to measure ambient temperature, and an anemometer (A100L2 from Vector Instruments) to measure wind speed. All monitored data are gathered at one-minute intervals using a calibrated data acquisition system (model MX100 with MX110-UNV-M10 modules from Yokogawa), which integrates the information from the different sensors and the operating voltage and current values for each PV module. In the specific case of the operating current, calibrated shunts (model Yokogawa 221508) are used to convert current into measurable voltage.

Finally, both the monitored data and the results of the simulations are analyzed and compared using data analysis and representation functions in R language. In this way, for each tested module configuration, statistical boxplots are generated by grouping monitored and simulated values according to different parameters, such as global irradiance level, wind speed or ventilation air mass flow. Furthermore, statistical parameters (averages, minimum, maximum, cumulative, etc.) are calculated and compared for the main parameters (power and temperature distribution of the module, air temperature and velocity through the channel, etc.). These values are then aggregated based on factors like time of day, irradiation level or air mass flow.

3 Results

3.1 Validation of the model through experimentation

A three-month experimental campaign is conducted during the summer of 2023 (from the 4th of July to the 9th of October) using the experimental setup described in Section 2.2. Figure 3 illustrates a photograph of the three installed modules (a) alongside an infrared thermographic image (b) taken at a moment of high irradiance (960 W/m^2). As expected, the thermographic image shows that the average temperature of the insulated module is higher than that of the other modules. It also reveals that the temperature of the module with the ventilation channel, with an air mass flow of 9.2 kg/min in that moment, increases along the air path. However, despite this increase, the maximum temperature reached remains lower than the temperatures observed in the other two modules.

The collected data are categorized based on similar meteorological conditions, with a primary focus on solar irradiance, ambient temperature, and wind speed. The thermal and electrical performance of the three modules is then analyzed under these specific conditions, enabling the identification of several phenomena. This way, Figure 4 illustrates some examples of statistical results obtained from the analysis of monitored data (channel height of 5 cm). First, it is observed that forced ventilation through the channel decreases the module temperature as expected, with this relative decrease being more pronounced at higher irradiance levels, reaching reductions up to 20 °C in the average module temperature (see Fig. 4a), when a constant air mass flow of 4.8 kg/min is applied. This reduction in the operating temperature leads to an increase in PV efficiency (greater than 1%, see Fig. 4b) and, consequently, an increase in the PV energy production of the module. Second, at a given irradiance level and wind speed, the module operating temperature consistently exceeds the ambient temperature by a certain constant offset. Third, increasing air mass flow results in a greater decrease in module temperature, although this improvement is not linear (see Fig. 4c). A balance between fan energy consumption and potential PV benefits must be considered. Additionally, a higher air mass flow rate results in a lower air temperature at the channel exit. Fourth, the

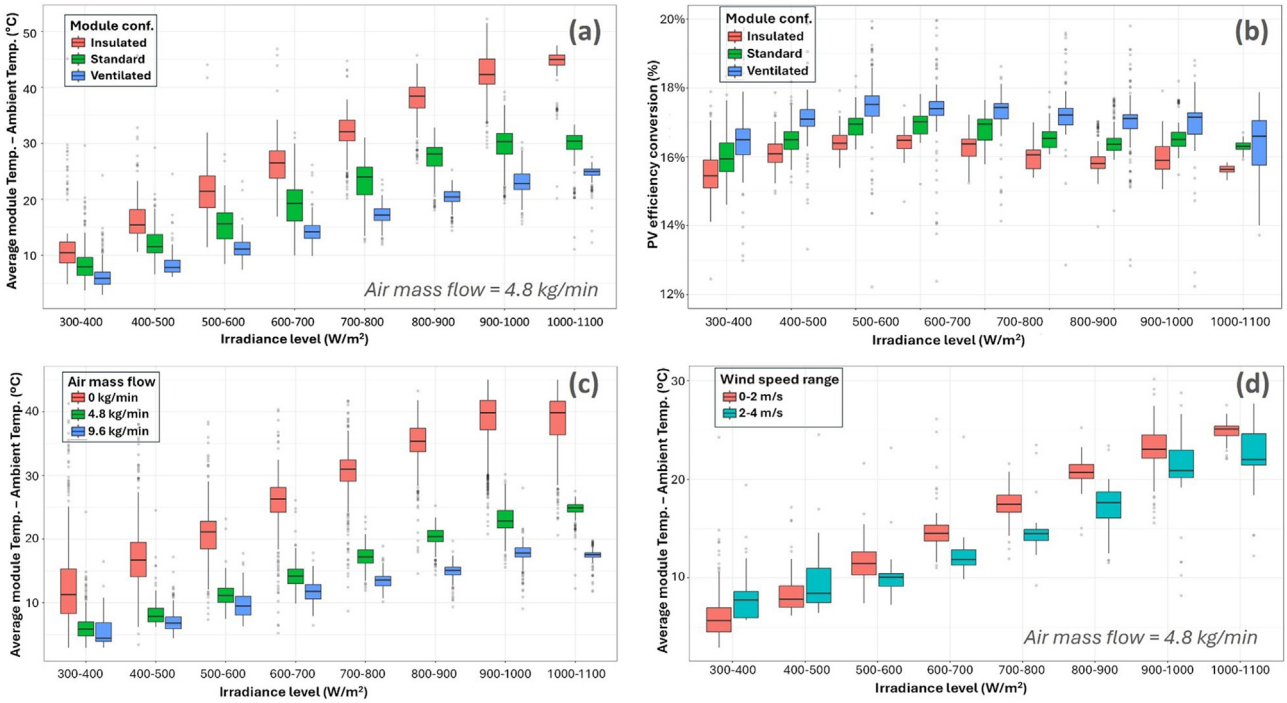

Fig. 4. Boxplots charts comparing experimental results of the three modules under study (M1, M2, M3), as a function of monitored global irradiance level: (a) Increase of modules temperature above ambient temperature; (b) PV efficiency conversion; (c) Increase of module M1 temperature above ambient temperature for different values of forced ventilated air mass flow, and (d) depending on the range of external wind speed.

decrease in the operating temperature of the ventilated module is lower when the external wind speed is high (see Fig. 4d). This is attributed to significant convective heat losses on the front side of the modules. In this way, in conditions of high wind speed values, the cooling from the front side of the module is significant, so the benefit of applying the rear-side cooling strategy is not so relevant.

The simulation model is adapted to the specific experimental setup, and meteorological data gathered during experimental campaign are used as input parameters to run simulations of the performance of the three modules over the monitored three-month period. A categorization and analysis of main simulated parameters, analogous to the one performed with experimental data, is conducted to achieve a direct comparison between simulated and experimental results. Key parameters evaluated for model validation include PV power production, module average temperature, and air temperature at the exit of the channel. During the monitoring campaign, key setup parameters, such as the ventilated air mass flow, are varied to validate the accurate operation of the simulation model with different configurations.

As an illustrative example, Figure 5 shows graphs comparing experimental and simulated results of key parameters during two representative days: a steady hot sunny day (August 23rd, 2023) with an air mass flow of 4.6 kg/min, and a partially cloudy day (September 12th, 2023) with fluctuating conditions and an air mass flow of 2.4 kg/min, both with 5 cm of channel height. There is a strong agreement between the simulated and experimental results, with high accuracy observed in all three parameters: PV power production, module average temperature, and air temperature at the channel exit.

Nevertheless, the model is not capable of simulating certain localized phenomena. For example, the thermographic image in Figure 3b shows unexpected dark areas on the module with the air channel, which correspond to real-world elements located behind the module, such as metallic frames or electrical boxes. These elements cause locally increased turbulence in the airflow, resulting in enhanced cooling. However, when considering average temperatures of both the module and the air at the exit of the channel, the model accurately predicts the overall thermal behavior of the entire setup.

In order to quantify the deviation of the model, Figure 5 also presents the boxplot charts showing the statistical distribution of the instantaneous relative error between simulated results and monitored data. As expected, the instantaneous deviation of the simulation results for the three parameters is higher during the day with more fluctuating meteorological conditions. Nevertheless, even under these fluctuating conditions, the average relative error throughout the day remains very low for each of the three analyzed parameters: −0.1% for module power, +0.4 °C for module temperature, and −0.3 °C for exit air temperature; with standard deviation values over the entire day reaching up 4.5%, 1.3 °C and 0.7 °C, respectively.

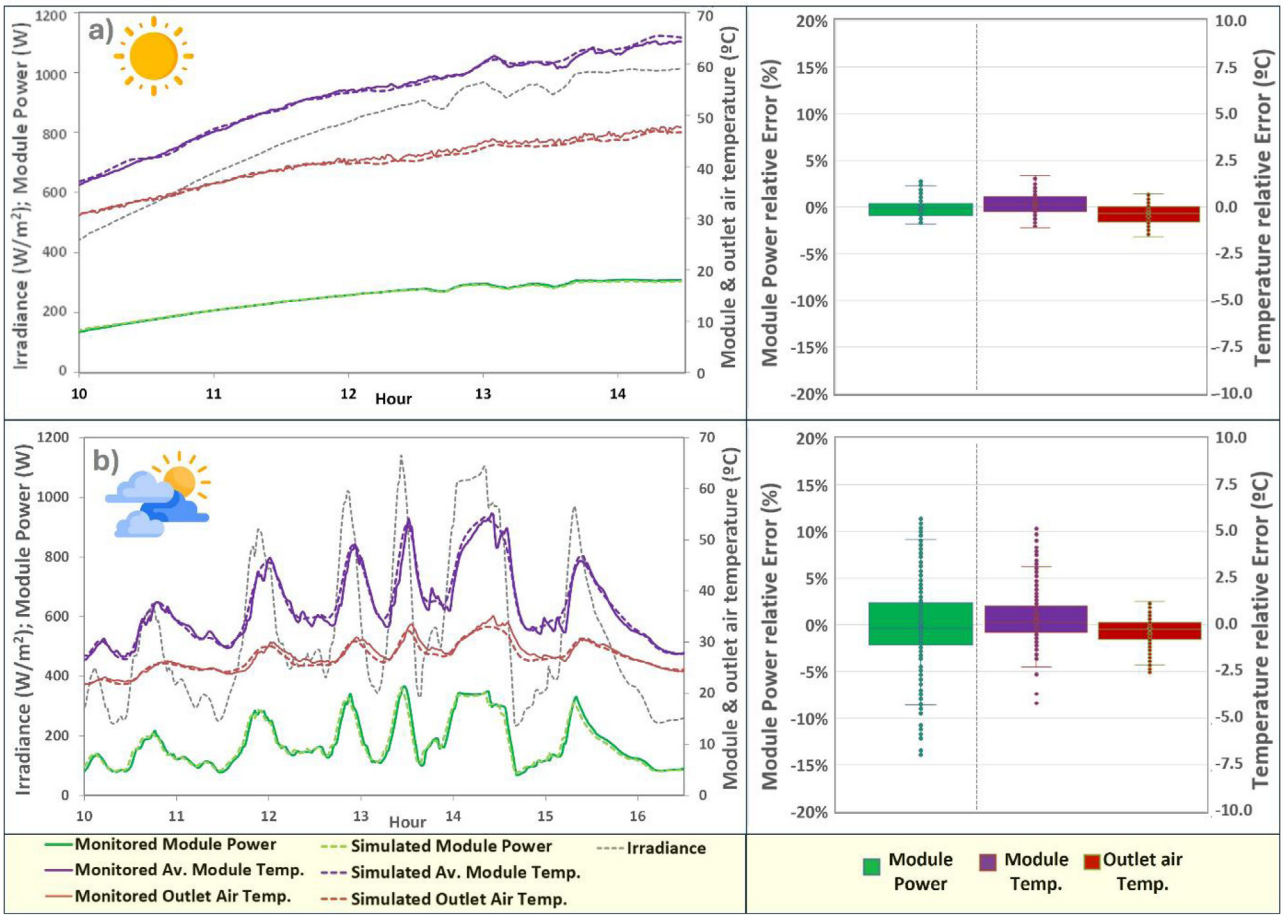

Fig. 5. Graphical comparison between main monitored and simulated results in the case of a clear sunny day (a) and a fast-changing clear-cloudy day (b), including boxplot charts with the statistical distribution of the instantaneous relative error.

3.2 Real case design and evaluation

Figure 6a presents a photograph of the current aspect of the IWER building, which serves as the real case study for this research. Figure 6b provides a digital image from the renovation project, illustrating the future appearance of the building. The subsequent subsections detail the results from the simulations conducted for the specific roof section under study, which is depicted in Figure 6c.

3.2.1 Preliminary simulations

Preliminary simulations focus on increasing PV energy generation using a ventilation channel compared to a conventional rooftop PV installation. In the initial stage, potential differences between constructing the air channel with PV modules in portrait or landscape configuration are evaluated. The differences in daily energy production for the selected roof are practically negligible for all considered cases (below 0.5%). Therefore, it is decided to proceed with the performance evaluation using modules in portrait orientation because this configuration is easier for their final assembly. Giving the dimensions of the selected roof-section, ventilation channels measuring 8.9 m in length and 1 m in width are designed, incorporating five Meyer Burger Black modules in portrait configuration (see Fig. 6).

These preliminary simulations also assess the impact of the channels height, testing heights ranging from 5 to 30 cm and air velocities through the channel from 0.5 to 5 m/s. Initially, constant air velocities are used throughout the year, which will be varied according to needs in subsequent simulations. As illustrated in Figure 7, a 10 cm channel height with an air velocity of 5 m/s resulted in a 4.6% increase in PV energy production during a Typical Meteorological Year (TMY) in Pamplona. Increasing the channel height from 5 to 10 cm at any given air velocity, leads to an annual PV energy production increase between 0.24% and 0.35%. This increase reaches daily peaks of 0.57% on sunny summer days. However, further increases in height beyond 10 cm do not yield significant improvements in PV energy production (less than 0.11% for all cases simulated), and even cause a slight decrease for heights greater than 20 cm. Consequently, a channel height of 10 cm is selected for subsequent simulations to optimize the design. Nonetheless, it is important to consider the trade-off between cost reduction (5 cm), and the maximization of PV energy production (10 cm). This balance will be addressed in the upcoming stages of this research.

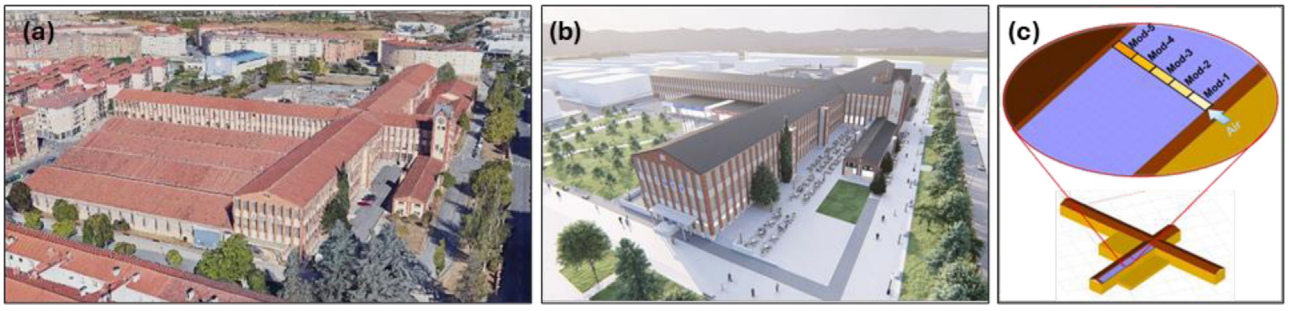

Fig. 6. (a) Aerial photograph of IWER building before renovation; (b) Digital image of future renovated IWER building (reproduced with permission of Obras Especiales); (c) Render of the building and roof section under study.

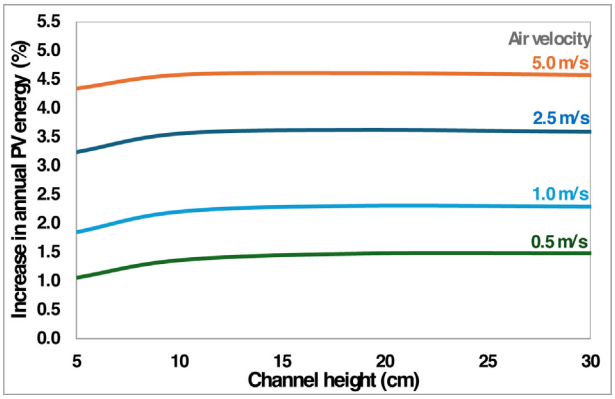

Fig. 7. Graph showing the annual increase in PV energy production versus the channel height for four different air velocities through a channel with five modules in portrait configuration.

In the following sections, different control strategies for the forced ventilation system will be compared, maintaining the same characteristics for the PV-T element: ventilation channels measuring 8.9 m in length, 1 m in width and 10 cm in height, incorporating five Meyer Burger Black modules in portrait configuration.

3.2.2 Linear control of fans

To adjust the air velocity according to cooling needs derived from ambient conditions, a linear control strategy for the fans is initially implemented based on the irradiance levels as the input control parameter. In this approach, the air velocity through the channel is proportionally increased with irradiance level, ranging from 0 m/s for irradiance levels below 50 W/m^2 to 3 m/s for an irradiance level of 1000 W/m^2. Using this configuration and a TMY of Pamplona as meteorological input, the gain in the net annual energy balance was 33.9 kWh per kW_p installed, resulting in an overall improvement of annual generated energy of 2.2%. The term kWh/kW_p, known as specific energy production, is a fair parameter for comparisons, as it is independent of the model and number of modules, size of the installation, and other variables.

Regarding the thermal behavior of the element, the difference between air temperature at the exit of the channel and the ambient temperature is also assessed. A non-linear increase with irradiance levels is observed, ranging from 2 °C at 50 W/m^2 up to 12 °C at 1100 W/m^2. In addition, an important decrease in the operating temperature of the modules was noted. The monthly module's temperature decrease in summer is around −7 °C in average, reaching values up to −33 °C during specific moments with high levels of irradiance. A summary of these results is shown in the graph of Figure 9 and in Table 4.

3.2.3 Four-step control of fans

Despite the promising performance of the described linear control strategy, it presents significant practical implementation challenges. This strategy would require a high-power fan with a Proportional-Integral (PI) controller capable of varying the fans rotational speed in real-time based on the monitored irradiance values. Several control strategies are initially evaluated to streamline implementation and try to reduce the total fan power consumption. Among these strategies, it is decided to deepen the analysis of a setup based on four low-power fans per channel, with each fan operating in a simple ON/OFF mode. This choice was made because it offers a good balance between easiness of implementation and performance.

The initial four-step control strategy configuration is based on the results of the linear control, selecting interval steps of 200 W/m^2 of irradiance as trigger values for the operation of the individual fans. In this way, no fan is active for irradiance below 200 W/m^2; the first fan is activated at 200 W/m^2; the second at 400 W/m^2; the third at 600 W/m^2; and all four fans operate for irradiance above 800 W/m^2, providing an air velocity of 3 m/s through the channel.

The analysis of the simulation results shows that this strategy increases the annual PV energy generation by only 0.6 kWh/kW_p. However, with this new strategy the annual fan energy consumption also significantly increases by 2.8 kWh/kW_p, resulting in a net annual energy balance of 31.7 kWh/kW_p, which implies a relative decrease of 6.3% compared to the initial linear control strategy. Therefore, to optimize the control strategy performance, a differential evolution algorithm is applied using the net annual energy balance as the figure of merit. The algorithm runs the model multiple times, combining and exploring different values of the selected variables under study, to determine the optimal values to maximize the net annual energy

Table 2. Variables chosen for the optimization, searching range (lower and upper limits), and optimal values obtained.

Variable to optimize	Lower limit	Upper limit	Optimal value
Channel height (cm)	5.0	11.0	9.6
Maximum air velocity (m/s)	1.50	2.50	2.11
Irradiance lower step (W/m^2)	75	200	96
Irradiance higher step (W/m^2)	600	750	687

Table 3. Control values of irradiance, and air velocity through the channel, for activation of the fans in the four-step initial and optimized control strategies.

4-step control strategy	1st step	2nd step	3rd step	4th step
Initial (W/m^2 – m/s)	200 – 0.75	400 – 1.50	600 – 2.25	800 – 3.00
Optimized (W/m^2 – m/s)	96 – 0.53	293 – 1.06	490 – 1.58	687 – 2.11

Table 4. Comparative summary of main results from the annual simulated data for the three forced-ventilation control strategies.

Control strategy	Linear	4-step	4-step Opt.
Δ PV Generated Energy (kWh/kWp)	48.5	49.2	44.0
Δ Fan Consumed Energy (kWh/kWp)	−14.7	−17.4	−8.2
Δ Net Energy Balance (kWh/kWp)	33.9	31.7	35.7
Δ PV Generated Energy (%)	3.1%	3.2%	2.8%
Δ Fan Consumed Energy (%)	−0.9%	−1.1%	−0.5%
Δ Net Energy Balance (%)	**2.2%**	**2.0%**	**2.3%**
Δ PV module T Average (°C)	−6.8	−6.7	−6.4
Δ PV module T Maximum (°C)	−33.0	−33.3	−31.6
Δ Air T Average at channel exit (°C)	6.2	6.7	8.1
Δ Air T Maximum at channel exit (°C)	13.1	17.4	20.0

balance. In this way, Table 2 summarizes the variables chosen for the optimization, their searching range (lower and upper limits), and the optimal values obtained. The channel height is also included as a variable to confirm the selection from preliminary simulations, which only considered PV energy production without considering the consumption of the fans. The optimal value obtained for this channel height is 9.6 cm, which is close enough to the initially selected 10 cm, considering potential practical deviations during implementation, validating the previously exposed simulated results. It is also important to note that during the optimization process the irradiance steps for turning the second and third fans ON/OFF are defined using equidistant irradiance intervals within the tested lower and upper limit values.

Table 3 features the values used for irradiance and air velocity through the channel for the four steps corresponding with the activation of each fan, for both initial and optimized control strategies.

According to equation (4), based on the geometry of a single ventilation channel, the air velocity from the optimized fourth step in Table 3, and assuming an efficiency of 50%, the estimated fan power rating per channel is approximately 16.8 W. This value is notably lower than the nominal PV power of the same channel, which consists of five modules of 385 W each, resulting in a total of 1.925 kW per channel. Furthermore, the analysis of the annual simulation results indicates that optimizing the conditions for activation of the fans significantly reduces their energy consumption, even in comparison with the linear strategy, with a reduction of 6.4 kWh/kW_p. However, this new control strategy also implies a slight decrease in PV energy production, with a reduction of 4.5 kWh/kW_p compared to the linear case. Despite this, the overall annual net energy balance increases to 35.7 kWh/kW_p, which represents a 2.3% annual growth compared to a conventional rooftop installation. These findings demonstrate that the optimized four-step control

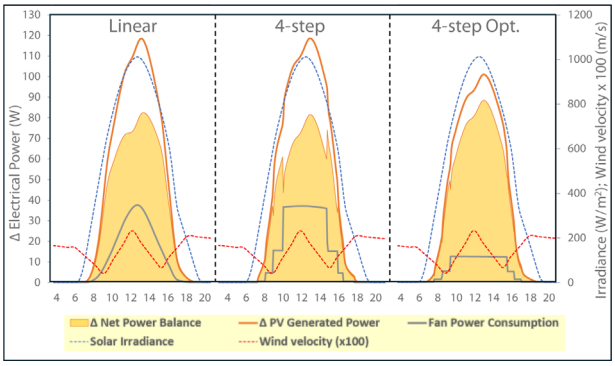

Fig. 8. Example of temporal evolution of solar irradiance, wind speed, and primary energy-related simulated results (increase in PV generated power due to ventilation; electrical power consumption of the fans; increase in net power balance), during a clear sunny summer day, for the three forced-ventilation control strategies under study.

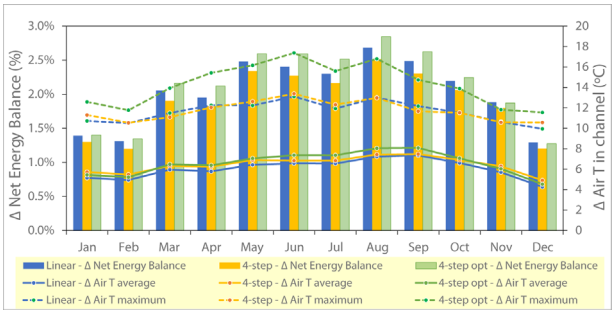

Fig. 9. Comparison of monthly evolution for the three ventilation control strategies under study: Percentage of monthly increase in net energy balance due to the forced ventilation (*bars*); Monthly average (*solid lines*) and maximum increase (*dashed lines*) of air temperature through the ventilation channel.

strategy leads to an improvement in the net annual energy balance, even compared to the linear strategy that is too complex to be implemented in practice. Table 4 and Figure 9 summarize these results.

3.2.4 Control strategies performance comparison

To compare the performance of the three forced ventilation control strategies tested, Figure 8 presents an illustrative example showing the temporal evolution of the key energy-related simulated results (increase in PV generated power due to ventilation; electrical power consumption of the fans; increase in net power balance), during a clear sunny summer day from the TMY of Pamplona. Moreover, the graphs include solar irradiance and wind speed values for comprehensive analysis.

Figure 9 illustrates the monthly net energy balance improvements for the three control strategies implemented throughout the TMY of Pamplona. Additionally, it shows the monthly average and maximum air temperature

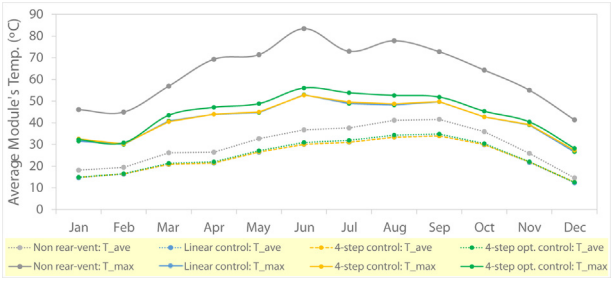

Fig. 10. Comparison of monthly average and maximum temperatures achieved by the PV modules with the standard non forced ventilation scheme, and the three different ventilation control strategies studied.

increase at the outlet of the forced ventilation channel compared to the ambient temperature. The optimized four-step control strategy provides the highest net generated energy values throughout the year, and the relative increase compared to the linear control strategy is more pronounced during the central months with higher irradiation. For instance, an increase in the net generated energy of up to 2.9% (5.3 kWh/kW_p) can be observed in August.

On the other hand, the increase of air temperature at the exit of the ventilation channel is also more pronounced during months with higher irradiation, as expected. The monthly average increase of the air temperature is quite similar for the three control strategies tested. However, the maximum values achieved by the optimized control strategy are significantly higher than those of the other strategies, reaching up to 17.4 °C in June. This increased air temperature in the optimized control strategy is due to a lower air mass flow in the ventilation channel under high levels of irradiance, compared with the other two strategies, which implies a smaller mass flow of warmer air at the outlet.

Figure 10 shows the monthly average daytime temperature reached by the modules with the conventional mounting setup and compares them with the three control strategies studied for the forced ventilation setup. Additionally, the maximum temperatures reached by the PV modules for these four setups are also shown in the graph. The reduction in the average module temperature is quite similar for the three control strategies, varying from 2 °C of cooling during the coldest months to approximately 7 °C during the sunniest months. Nevertheless, due to the strategy of increasing the air velocity through the channel as irradiance levels rise, the reduction in the module temperature during periods of high irradiance is significantly greater. Consequently, by applying any of the three ventilation strategies, the maximum operating temperature of the modules can be reduced by more than 30 °C during months with higher irradiance. This is an important additional benefit of the devised element, since it prevents the modules from operating at temperatures exceeding 56 °C, thereby extending their lifespan. This is further discussed in the upcoming section.

Finally, as a comparative summary, Table 4 shows the most significant results extracted from the analysis of the annual simulated data for each of the three forced-ventilation control strategies studied. Data shown in the table are variations relative to the annual values obtained for the simulation of a conventional rooftop PV installation.

4 Discussion

The developed PV-T simulation model has been experimentally validated using a commercial PV module under diverse weather conditions, air velocities through the ventilation channel, channel heights, etc. The model can simulate the electrical and thermal behavior of any PV system configuration incorporating this forced ventilation, including BAPV-T and BIPV-T elements, at any location. While the results presented in this paper are specific to a particular installation (IWER building in Pamplona, southeast oriented roof section, Meyer Burger Black modules, five modules on portrait configuration per channel section, etc.), similar studies can be conducted for other locations and system configuration, in order to determine optimal settings for easy implementation and estimate the net energy benefits under new conditions.

Consistent with observations made during the experimental campaign, the simulations of the IWER building roof revealed that the improvement in PV energy production is lower at high values of external wind speed due to significant front-side cooling. Although the influence of wind speed is not as significant as that of the irradiance level, it is substantial enough to be considered. Thus, next steps of this research will include the implementation of wind speed as a new variable in the fan control strategy. This would need the incorporation of an anemometer on or near the building for real-time wind speed monitoring, which would increase installation complexity and costs. However, this upgrade is expected to improve the net energy balance, so its feasibility will be assessed accordingly.

Moreover, in this work the four-step control strategy has been optimized for the complete year. However, implementing different trigger values for each step control strategy based on the time of the year could further improve the net annual energy balance. For instance, the same physical setup but different control parameters could be used in two different configurations depending on the season (summer and winter modes of ventilation). In future steps, the optimization algorithms will be used to determine the optimal values to maximize the net energy increment each month, employing this variable control strategy throughout the year.

Future work will also include the application of this methodology to identify the best control strategy for other conditions: latitude of the installation, tilt angle and orientation of the roof, different PV module technology, channel heights, etc. The specific PV module used in the experimental and simulation tests (Meyer Burger Black) has been initially selected within the oPENLab project. This module is based on silicon heterojunction (HJT) technology PV cells, which have a maximum power temperature coefficient ($\gamma = -0.259\%/°C$) significantly lower than PV modules based on other silicon technologies (typically between $-0.30\%/°C$ and $-0.37\%/°C$). Thus, using this forced ventilation methodology with PV modules with higher absolute temperature coefficients will increase the relative benefit in the net energy balance compared to the results obtained for these HJT PV modules under study.

In addition to increasing the PV energy production, the implementation of the proposed ventilation strategy also prevents the PV modules from operating at high temperatures, extending significantly their durability and lifespan. This additional benefit is particularly important for these more challenging-to-replace BAPV-T or BIPV-T systems. In this way, this behavior is highlighted by the International Energy Agency in the task 15 of the PV Power Systems (IEA-PVPS) program [25], where it is clearly established that extending the durability of PV modules is crucial for the widespread adoption of BIPV systems, because these modules will normally be subjected to much more severe operating conditions than the PV modules in a standard utility scale installation. Consequently, the potential long-term benefits associated with this significant reduction in operating temperature of the modules will be considered in future stages of the system assessment.

Furthermore, potential uses of the warm air at the channel exit will be also evaluated, assessing its benefits for space heating and supporting domestic hot water production with the aim of a more integrated approach. To achieve this, the model will be adapted to account for piping and systems pressure drop, which may influence the optimal design parameters such as channel height and air mass flow rates. While these adaptations may enhance the benefits of utilizing warm air, they could potentially impact PV module cooling and the associated increase in PV energy production. For this reason, a new figure of merit combining both thermal and PV-related benefits to optimize the control strategy will be needed, since the one utilized in the current study is focused on PV improvements. Seasonal variations will be also considered, enabling the development of strategies to switch from using the warm air for building applications to solely cooling the PV modules.

In summary, the optimal use of the warm air generated through the ventilation channel will depend on a variety of factors: type of climate, heating system of the building, layout of the air piping system, etc. For instance, in very cold climates, the use of the generated warm air for space heating might be extended over a significant part of the year. In this line, exploiting the ease of implementation of the proposed element, locations with a broad range of climatic conditions will be also simulated optimizing the parameters of the control strategies. This way, apart from confirming the foreseen replicability of the element in different locations, an assessment of the climatology where the system will be most favorable will be performed.

In the line of integrating PV in buildings, utilizing these PV modules as rainscreen similar to ventilated façades and incorporating the produced warm air into the building facilities, exemplifies an easily implementable BIPV-T

system. A complete economic assessment will be also conducted, comparing the estimated benefits in the net annual energy balance, including thermal energy from the use of warm air, and in modules lifespan extension, with the increased installation costs compared to a conventional rooftop installation.

5 Conclusions

A comprehensive model has been developed and experimentally validated to accurately predict the thermal and electrical performance of air-based PV-T elements from a PV point of view. The model is highly versatile and can be easily applied to multiple locations, climatic conditions and element configurations, including those implemented in buildings such as BAPV-T or BIPV-T systems, to find the best design and control parameters.

An easily implementable element is proposed, utilizing a narrow air ventilation channel (height from 5 cm to 10 cm) directly formed between the back side of the PV modules and the top side of the roof. The system is analogous to the rainscreen in ventilated façades, a well-known approach in BIPV.

Specifically, simulation results of this element integrated on a section of the roof of the IWER building in Pamplona have been presented. Using this case study and a TMY for this location, different fan control strategies to provide the forced ventilation through the channel have been tested, based on the irradiance level as input control parameter. Outcomes in terms of net annual energy balance, PV modules operating temperature, and air temperature at the channel exit have been presented for three different fan control strategies: linear control, four-step control and four-step control with optimized trigger values for each step.

The optimized four-step ventilation control strategy exhibits the best performance in terms of net annual energy balance, achieving a 2.3% increase compared to a conventional rooftop installation. Although the increase in PV energy production is slightly lower than that of the other strategies, the energy consumption of the fans is also significantly reduced. In terms of thermal performance, the maximum reduction in operating module temperature using this control strategy has reached 31.6 °C, with an annual average reduction of 6.4 °C. Additionally, the air temperature at the channel exit is increased above the ambient temperature by an annual average of 8.1 °C, with maximum increments reaching 20 °C.

Most of the numerical results shown during the article correspond to the study of a particular case, but the versatility of the implemented simulation model allows finding the best design and control parameters of the air channel for the active cooling of the PV modules, for any desired condition (location, roof inclination, PV module model, etc.).

The results presented in this paper demonstrate the feasibility of using this type of active module cooling strategy in BIPV or BAPV installations. This approach aims to achieve the triple objective of maximizing net green energy production, extending the lifespan of PV modules, and recovering hot air, which can be utilized to reduce the overall energy consumption of the building.

Acknowledgments

Authors would like to acknowledge Roberto Astiz and Ibai Abentin for their invaluable work and technical support on the construction of the experimental setup and during the monitoring campaign.

Funding

This research was funded by the European Union's Horizon 2020 research and innovation program under grant agreement No. 101037080 (oPEN Lab project). The sole responsibility for the content of this document lies with the authors. It does not necessarily reflect the opinion of the European Union. Neither CINEA nor the European Commission are responsible for any use that may be made of the information contained herein.

Conflicts of interest

The authors have nothing to disclose.

Data availability statement

Further data generated within this research are confidential.

Author contribution statement

Conceptualization, M.E. and F.Z.; Methodology, I.C., M.E., P.S. and F.Z.; Software, I.C., P.S. and F.Z.; Validation, I.C., M.E. and P.S.; Formal Analysis, I.C. and M.E.; Investigation, I.C. and M. E.; Data Curation, M.E.; Writing – Original Draft Preparation, I. C., M.E., G.D. and F.Z.; Writing – Review & Editing, I.C., M.E., A.K., G.D., O.I. and F.Z.; Visualization, I.C. and M.E.; Project Administration, A.K. and O.I. All authors have reviewed, discussed, and agreed to their individual contributions.

References

1. REN21. Renewables 2023 global status report. A comprehensive annual overview of the state of renewable energy
2. T.E. Kuhn, C. Erban, M. Heinrich, J. Eisenlohr, F. Ensslen, D.H. Neuhaus, Review of technological design options for building integrated photovoltaics (BIPV), Energy Build. **231**, 110381 (2021). https://doi.org/10.1016/j.enbuild.2020.110381
3. M. Herrando, K. Wang, G. Huang, T. Otanicar, O.B. Mousa, R.A. Agathokleous, Y. Ding, S. Kalogirou, N. Ekins-Daukes, R.A. Taylor, C.N. Markides, A review of solar hybrid photovoltaic-thermal (PV-T) collectors and systems, Prog. Energy Combust. Sci. **97**, 101072 (2023). https://doi.org/10.1016/j.pecs.2023.101072

4. S.S. Joshi, A.S. Dhoble, Photovoltaic –Thermal systems (PVT): Technology review and future trends, Renew. Sustain. Energy Rev. **92**, 848 (2018). https://doi.org/10.1016/j.rser.2018.04.067
5. K. Wang, M. Herrando, A.M. Pantaleo, C.N. Markides, Technoeconomic assessments of hybrid photovoltaic-thermal vs. conventional solar-energy systems: Case studies in heat and power provision to sports centres, Appl. Energy **254**, 113657 (2019). https://doi.org/10.1016/J.APENERGY.2019.113657
6. International Renewable Energy Agency (IRENA), Power to heat and cooling: Status and pace of progress (2023). Retrieved from https://www.irena.org/Innovation-landscape-for-smart-electrification/Power-to-heat-and-cooling/Status
7. S.M. Sultan, M.N. Ervina Efzan, Review on recent Photovoltaic/Thermal (PV/T) technology advances and applications, Sol. Energy **173**, 939 (2018). https://doi.org/10.1016/j.solener.2018.08.032
8. M. Farshchimonfared, J.I. Bilbao, A.B. Sproul, Full optimisation and sensitivity analysis of a photovoltaic–thermal (PV/T) air system linked to a typical residential building, Sol. Energy **136**, 15 (2016). https://doi.org/10.1016/J.SOLENER.2016.06.048
9. E.D. Rounis, A.K. Athienitis, T. Stathopoulos, Multiple-inlet Building Integrated Photovoltaic/Thermal system modelling under varying wind and temperature conditions, Sol. Energy **139**, 157 (2016). https://doi.org/10.1016/J.SOLENER.2016.09.023
10. J.G. Ahn, J.H. Kim, J.T. Kim, A Study on Experimental Performance of Air-Type PV/T Collector with HRV, Energy Procedia **78**, 3007 (2015). https://doi.org/10.1016/J.EGYPRO.2015.11.705
11. N. Aste, G. Chiesa, F. Verri, Design, development and performance monitoring of a photovoltaic-thermal (PVT) air collector, Renew. Energy **33**, 914 (2008). https://doi.org/10.1016/J.RENENE.2007.06.022
12. A. Tiwari, M.S. Sodha, Parametric study of various configurations of hybrid PV/thermal air collector: Experimental validation of theoretical model, Sol. Energy Mater. Sol. Cells **91**, 17 (2007). https://doi.org/10.1016/J.SOLMAT.2006.06.061
13. J.K. Tonui, Y. Tripanagnostopoulos, Performance improvement of PV/T solar collectors with natural air flow operation, Sol. Energy **82**, 1 (2008). https://doi.org/10.1016/J.SOLENER.2007.06.004
14. Y. Jia, G. Alva, G. Fang, Development and applications of photovoltaic–thermal systems: A review, Renew. Sustain. Energy Rev. **102**, 249 (2019). https://doi.org/10.1016/J.RSER.2018.12.030
15. M. Herrando, C.N. Markides, Hybrid PV and solar-thermal systems for domestic heat and power provision in the UK: Techno-economic considerations, Appl. Energy **161**, 512 (2016). https://doi.org/10.1016/J.APENERGY.2015.09.025
16. M. Samykano, Hybrid Photovoltaic Thermal Systems: Present and Future Feasibilities for Industrial and Building Applications, Buildings **13**, 1950 (2023). https://doi.org/10.3390/buildings13081950
17. V.V. Tyagi, N.L. Panwar, N.A. Rahim, R. Kothari, Review on solar air heating system with and without thermal energy storage system, Renew. Sustain. Energy Rev. **16**, 2289 (2012). https://doi.org/10.1016/j.rser.2011. 12.005
18. S.E. Mattsson, H. Elmqvist, Modelica – An International Effort to Design the Next Generation Modeling Language, IFAC Proc. **30**, 151 (1997). https://doi.org/10.1016/s1474-6670(17)43628-7
19. L.R. Petzold, Description of DASSL: a differential/algebraic system solver, in *10th IMACS World Congress* (United States, 1982)
20. ≪Dymola≫, Dassault Systèmes. Available in: https://www.3ds.com/products/catia/dymola
21. ≪Open-Source-Modelica-Consortium, 2013 OpenModelica – An opensource Modelica-based modeling and simulation environment≫. Available https://openmodelica.org/
22. R. Franke, F. Casella, M. Sielemann, K. Proelss, M. Otter, M. Wetter, Standardization of Thermo-Fluid Modeling in Modelica. Fluid, in *7th Modelica Conference* (Como, Italy 2009)
23. V.V. Gnielinski, Neue Gleichungen fuer den Waerme- und den Stoffuebergang in turbulent durchstroemten Rohren und Kanaelen, Forsch. Ing.-Wes. **41**, 8 (1975)
24. W. Salameh, C. Castelain, J. Faraj, R. Murr, H. El, M. Hage, Improving the efficiency of photovoltaic panels using air exhausted from HVAC systems: Thermal modelling and parametric analysis, Case Stud. Therm. Eng. **25**, 100940 (2021). https://doi.org/10.1016/j.csite. 2021.100940
25. IEA, Enabling Framework for the Development of BIPV. https://iea-pvps.org/research-tasks/enabling-framework-for-the-development-of-bipv/

Cite this article as: Iñaki Cornago, Mikel Ezquer, Francisco Javier Sorbet, Alicia Kalms, Gonzalo Diarce, Olatz Irulegi, Fritz Zaversky, New approach of PV and thermal modeling to develop feasible cooling solutions for PV in buildings, EPJ Photovoltaics **16**, 19 (2025), https://doi.org/10.1051/epjpv/2025007